Article

Mechanical Amplification Exhibited by Quiescent Saccular Hair Bundles

Yuttana Roongthumskul[1] and Dolores Bozovic[1,2,*]
[1]Department of Physics and Astronomy and [2]California NanoSystems Institute, University of California, Los Angeles, Los Angeles, California

ABSTRACT Spontaneous oscillations exhibited by free-standing hair bundles from the Bullfrog sacculus suggest the existence of an active process that might underlie the exquisite sensitivity of the sacculus to mechanical stimulation. However, this spontaneous activity is suppressed by coupling to an overlying membrane, which applies a large mechanical load on the bundle. How a quiescent hair bundle utilizes its active process is still unknown. We studied the dynamics of motion of individual hair bundles under different offsets in the bundle position, and observed the occurrence of spikes in hair-bundle motion, associated with the generation of active work. These mechanical spikes can be evoked by a sinusoidal stimulus, leading to an amplified movement of the bundle with respect to the passive response. Amplitude gain reached as high as 100-fold at small stimulus amplitudes. Amplification of motion decreased with increasing amplitude of stimulation, ceasing at ~6–12 pN stimuli. Results from numerical simulations suggest that the adaptation process, mediated by myosin 1c, is not required for the production of mechanical spikes.

INTRODUCTION

Mechanical sensitivity of vestibular and auditory detection routinely reaches into the subnanometer regime (1,2). The detection is performed by hair cells, biological sensors that transduce displacements of hair bundles induced by vibrations into changes in the membrane potential. This process of mechanoelectrical transduction in turn allows the signal to be transmitted to the brain. Estimates of the passive properties of a hair bundle indicate that its noise floor, mainly originating from thermal fluctuations in water and channel gating stochasticity, should be significantly higher than the detection threshold (1,3). How the transduction process mediated by hair bundles overcomes the effects of noise to achieve its extreme sensitivity remains an open problem.

Hair cells of the inner ear have been shown to exhibit active processes, including somatic and/or bundle motility, depending on the species (4). In the mammalian cochlea, this active process is largely attributable to the protein prestin in the lateral membranes of outer hair cells (5). Hair bundles can generate an active force in response to mechanical stimulation (6,7). Under appropriate conditions, hair bundles of certain nonmammalian vertebrates, including those of the bullfrog sacculus, can exhibit spontaneous limit-cycle oscillations (8,9), one of the manifestations of an underlying active amplifier within the bundles. The active process has been shown to lead to a highly nonlinear response in induced hair-bundle deflection (10,11), and to be necessary for achieving extreme sensitivity (12,13).

When hair bundles are deflected by sound waves, tip links connecting the individual stereocilia are placed under tension, leading to the opening of mechanically sensitive ion channels. Gating of the transduction channels in the stereocilia leads to bistability in the position of the bundle, corresponding to channel opening and closing states. An adaptation process, mediated by an array of myosin motors physically connected to the transduction complex, continuously adjusts the position of the bundle. Significant noise is evident in this innate motility, with variation in the local frequency and phase of the oscillation. External signals of much smaller amplitude have been shown to entrain the spontaneous motion (14,15).

Theories based on nonlinear dynamics have been proposed to describe active hair-bundle motility (16–18). Higher-order nonlinearities have been shown to lead to rich bifurcation diagrams in the phase space. Dependent on the internal parameters, the auditory system could be poised near a number of different bifurcations, which determine the characteristics of its phase-locking to the applied stimulus. The theoretical models describe the nonlinear response observed experimentally, and predict the amplification of low-amplitude stimuli. In a recent study, we showed that at low amplitudes of an imposed sinusoidal drive, phase-locking of spontaneously oscillating bundles occurs via a saddle-node bifurcation, characterized by the occurrence of phase slips, sudden excursions of 2π, at a rate that is dependent on the amplitude and detuning of the applied drive (15). We measured the occurrence of phase slips in the response of the hair bundle and showed that the dynamics of the observed behavior were consistent with the stochastic Adler equation (19).

Under natural conditions, hair bundles of the bullfrog sacculus are coupled to an overlying otolithic membrane

Submitted August 28, 2014, and accepted for publication November 6, 2014.

*Correspondence: bozovic@physics.ucla.edu

Editor: E. Ostap.

0006-3495/15/01/0053/9 $2.00

http://dx.doi.org/10.1016/j.bpj.2014.11.009

(20,21). In preparations that maintained this coupling, hair bundles were shown not to exhibit spontaneous oscillations, indicating that loading can tune them across the bifurcation (22). Our observations indicated that attachment to the membrane may impose an offset on the position of the bundle with respect to its freestanding state. We hence explored the effects of an imposed mechanical deflection and found it to strongly affect the dynamic state of the bundle. Active oscillations can be suppressed by the application of an offset, with the transition displaying either frequency or amplitude modulation or an admixture of the two. In a high-calcium environment, a quiescent hair bundle can also exhibit spontaneous motion in response to deflection (23).

In this article, we explore the dynamic response of hair bundles deflected toward the kinocilium until suppression of spontaneous oscillation is achieved. To capture the regime where the system is quiescent, but still poised in the vicinity of the bifurcation, we apply gradual ramps or sequential steps to the positions of the hair bundles. We observe the occurrence of spikes—sudden and rapid excursions of the hair-bundle motion—under a range of imposed deflections. These spikes are stochastic, but are readily phase-locked by an imposed sinusoidal stimulus. We demonstrate that this spiking regime leads to a significant amplification of the signal and explore its mechanisms with a numerical simulation.

MATERIALS AND METHODS

Biological preparation

All animal-handling protocols were approved by the University of California Los Angeles Chancellor's Animal Research Committee (Protocol Number ARC 2006-043-13C) in accordance with federal and state guidelines. Sacculus from the inner ear of the North American Bullfrog (*Rana catesbeiana*) was excised in artificial perilymph, containing 110 mM Na^+, 2 mM K^+, 1.5 mM Ca^{2+}, 113 mM Cl^-, 3 mM d-glucose, 1 mM sodium pyruvate, 1 mM creatine, and 5 mM HEPES. The preparation was mounted into a two-compartment chamber, with the apical side immersed in artificial endolymph (2 mM Na^+, 118 mM K^+, 0.25 mM Ca^{2+}, 118 mM Cl^-, 3 mM d-glucose, and 5 mM HEPES) and the basal side in perilymph. The otolithic membrane was gently lifted off with an eyelash tool after 8-min enzymatic dissociation with 50 μg/mL Collagenase IV (Sigma Aldrich, St. Louis, MO).

Imaging and tracking of bundle motility

Preparations were imaged under an upright optical microscope (B51X, Olympus, Center Valley, PA). The images were magnified to ~400× and recorded at 500 frames/s by a high-speed complementary metal oxide semiconductor (CMOS) camera (Photron FASTCAM SA1.1). The hair bundle motion was tracked with software written in MATLAB (The MathWorks, Natick, MA). In each frame, the center of gravity of the intensity profile of the bundle was extracted as the center position. Intensity profiles of 15–20 vertically adjacent rows were tracked and averaged to improve the signal/noise ratio. The noise levels in the recordings were ~3–5 nm.

Mechanical stimulation

A borosilicate glass fiber was pulled with a micropipette puller (P97, Sutter Instruments, Novato, CA), with an additional rod 1 μm in diameter fabricated at a 90° angle using a microforge. The stiffness of the glass fiber was calibrated by fitting a Lorentzian function to the power spectral density of the fiber's Brownian motion in water, imaged at 10,000 frames/s. The stiffness of the fibers used in these experiments was 150–200 μN/m. A fiber was then mounted on a piezoelectric stimulator (P-150, Piezosystem Jena, Hopedale, MA) and attached to a hair bundle at the kinociliary bulb with a micromanipulator. Before the experiment, the fiber tip was dipped into 2 mg/mL concanavalin-A to enhance the adhesion. Slow ramps or step deflections were generated with a function generator (AFG 3022, Tektronix, Portland, OR) and sent to the piezoelectric amplifier. We explored the effects of deflection toward the kinocilium, mimicking the offset observed under the otolithic membrane. The ramp amplitude at the base of the fiber was fixed at 1.3 μm, reached over a 1-min period, and the step deflection was fixed at a maximum of 0.7 μm. Unless indicated otherwise, the offset reported is the absolute deflection at the tip of the bundle, whereas the sinusoidal amplitude is reported as the signal amplitude applied to the base of the probe.

Data analysis

Slow offsets in the bundle motion were removed from the data obtained from experiments with slow ramps, so the channel opening state fluctuates around zero. The traces were divided into sections 1-s long. The histogram of the bundle position of each section was calculated, and peaks of the histograms corresponding to the channel opening position were fit with a quadratic polynomial. This value was subtracted from the raw trace, defining zero position as that of the channel opening state.

A spike detection procedure was applied to the ramp-subtracted traces. A Gaussian distribution was fit to the histogram of the bundle position around the channel opening state to determine the standard deviation of the distribution. To ensure that the detected spikes are well above the noise level, a threshold was chosen to be 4 times this standard deviation. Any excursion of the bundle beyond the threshold was defined to be a spike. The number of spikes detected was found to be robust against small variation of the threshold (Fig. S1 in the Supporting Material). This threshold was fixed for all of the applied bundle offsets.

If sinusoidal stimuli were applied, the passive response of the bundle was removed before applying spike detection software. The passive response was determined by fitting a sine wave at the stimulus frequency to the bundle motion, ignoring any displacements >10 nm in the negative direction.

Once spikes were detected, their amplitudes were defined as the absolute minima of the excursions. The spike duration was defined as the interval between the two adjacent threshold crossings, thus slightly underestimating the full spike duration. Spike phase was defined as the phase of the stimulus cycle at the instant when the bundle motion crosses the threshold away from the channel opening state.

RESULTS

We studied the response of hair bundles subject to various degrees of steady-state deflection and sinusoidal stimuli of different amplitudes and frequencies. A flexible glass fiber was used to apply a static or a slowly increasing force toward the kinocilium, with a superposed sinusoidal signal. Hair bundles were found to exhibit spikelike motions under intermediate deflections.

Effects of mechanical offset on hair bundle oscillations

Under in vitro conditions, decoupled hair bundles from the Bullfrog sacculus typically exhibit spontaneous oscillations,

with comparable durations spent in the channel opening and closing states. To capture the behavior of hair bundle oscillations at different deflections, a ramp of linearly increasing offset was applied to the base of the glass fiber attached to the bundle. The ramp speed at the base of the fiber was chosen to be 22 nm/s, which is slow with respect to the rate of adaptation (24).

As the bundle was gradually deflected toward the kinocilium (defined to be the positive direction), hair-bundle motion exhibited two qualitatively different behaviors. At small to moderate offsets, an increase in the oscillation frequency was observed, together with a decrease in the amplitude of oscillation. Under larger deflections, a significant fraction of the hair bundles studied showed a spiking regime, during which the oscillations became increasingly asymmetric, favoring the channel opening state, and exhibited only brief excursions in the negative direction, away from the kinocilium (Fig. 1 *A*). The rate of occurrence of these observed spikes thus decreased under applied offset, until the motion was completely suppressed, as shown in Fig. 1 *B*. As a result, the ratio of the channel-closing to channel-opening intervals monotonically decreased. In this study, the spiking regime was defined to be the regime in which this ratio was <20%. This corresponded to the regime where the spike rate decreased as a function of offsets. Thus, as shown in Fig. 1 *B*, the onset of the spiking regime occurred when the spike rate reached its maximum (Fig. S2).

The mechanical spikes also demonstrated a gradual reduction in the amplitude (Fig. 1 *C*) and a decrease in the duration (Fig. 1 *D*). This reduction in amplitude was also observed in recordings obtained at a higher frame rate (2000 frames/s) and thus was not due to undersampling (Fig. S3). Spike durations were as short as 10 ms, indicating that a spiking bundle has an inherent ability to undergo one-to-one phase locking up to 100 Hz.

Note that some fraction of hair bundles did not exhibit the asymmetric oscillation profile under positive deflection. Instead, the oscillation became more rapid and decreased in amplitude until it vanished into the noise floor of the recording. This variation in the spontaneous motility under large offsets may imply two distinct subpopulations of hair bundles in the bullfrog sacculus. However, preliminary observations (measured in 15 cells) indicated no correlation

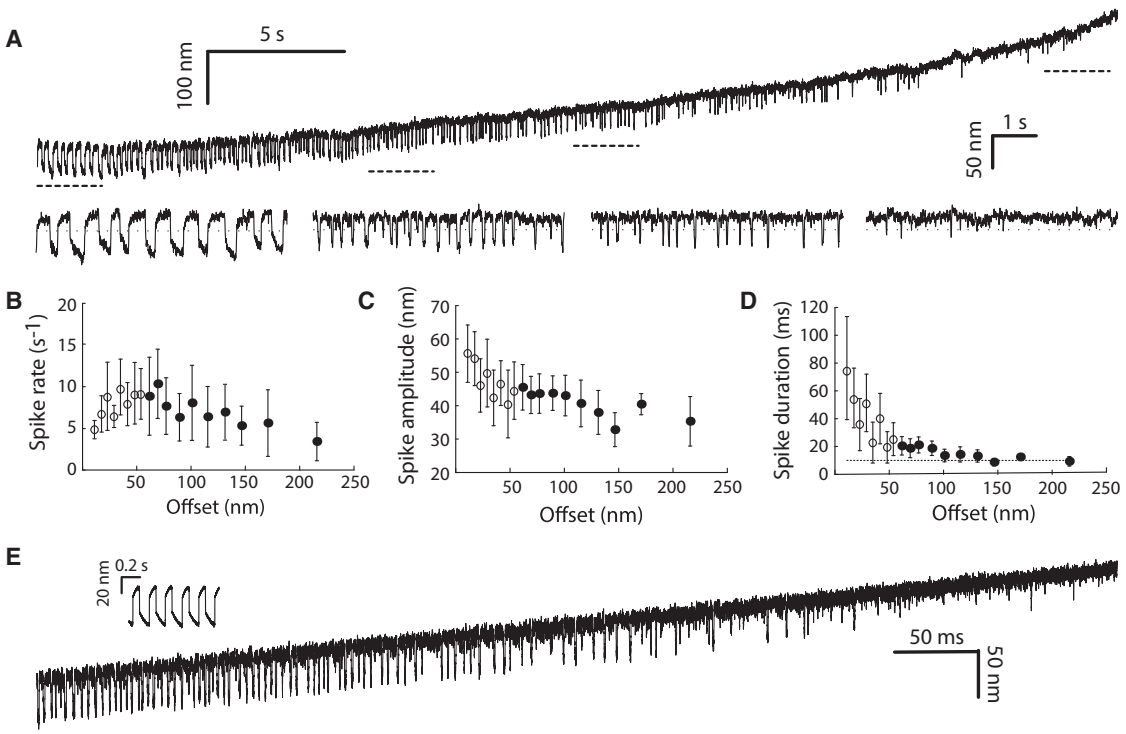

FIGURE 1 Characteristics of the spiking regime. (*A*) Spontaneous oscillations of a hair bundle under a slowly increasing positive offset (22 nm/s). Lower traces are the zoom-ins of four different sections of the full trace highlighted by dashed lines. Dotted lines indicate the threshold used for spike detection, corresponding to 4 times the standard deviation obtained from a histogram of the bundle position. (*B*) Rate of oscillation (*open circles*) and spike rate (*solid circles*). The rate showed a peak at the end of the oscillating regime, and decreased in the spiking regime. (*C*) Peak-to-peak amplitude of bundle motion as a function of the bundle offset in the oscillating (*open circles*) and spiking (*solid circles*) regimes. (*D*) Duration of bundle movement in the channel-closing state in the oscillatory (*open circles*) and spiking (*solid circles*) regimes, plotted at different bundle offsets. In the spiking regime, the duration saturated at ~10 ms. Each point in *B–D* represents the averaged value obtained from 10 successive spikes, and the error bars are the standard deviation. (*E*) Numerical simulations of spontaneous oscillations of a hair bundle under a slowly ramped offset. (*Inset*) Spontaneous oscillations obtained from the same set of parameters with no additional offset.

between the spiking behavior and the morphology of hair cells, which was previously shown to fall into two different subgroups (25). We focus here on hair bundles exhibiting robust spiking under deflection.

Hair-bundle response at different deflections

We next superposed sinusoidal stimuli onto the offsets. The stimulus frequency was chosen to match the characteristic frequency of the bundle oscillation at zero offset. In the spontaneously oscillating regime, the imposed signal entrained the innate motion (0 nm offset in Fig. 2 *A*). The phase-locking behavior gradually transitioned from one-to-one mode-locking to higher-order mode-locking as the characteristic frequency of the oscillation increased due to larger deflections (Fig. 2 *A*, *100-nm offset*).

As the bundles transitioned from the oscillatory to the spiking regime, they exhibited spikes superposed onto a passive response to the imposed sinusoidal stimulus (Fig. 2 *A*, *280-* and *350-nm offsets*). Amplitudes of the spikes decreased with offset (Fig. 2 *B*), whereas the passive response remained constant. For the particular experiment shown, spike amplitude was as large as ~10 times that of the passive response. This provides a potential mechanism for mechanical amplification by a hair bundle rendered quiescent by an imposed load.

Upon further deflection, spikes showed an increased probability of occurrence at a preferential phase within the stimulus cycle. This was illustrated by a rapid increase in the vector strength of the spike phase (Fig. 2 *D*). The averaged spike phase at large offsets saturated at ~$3\pi/2$, corresponding to the minimum of a stimulus cycle.

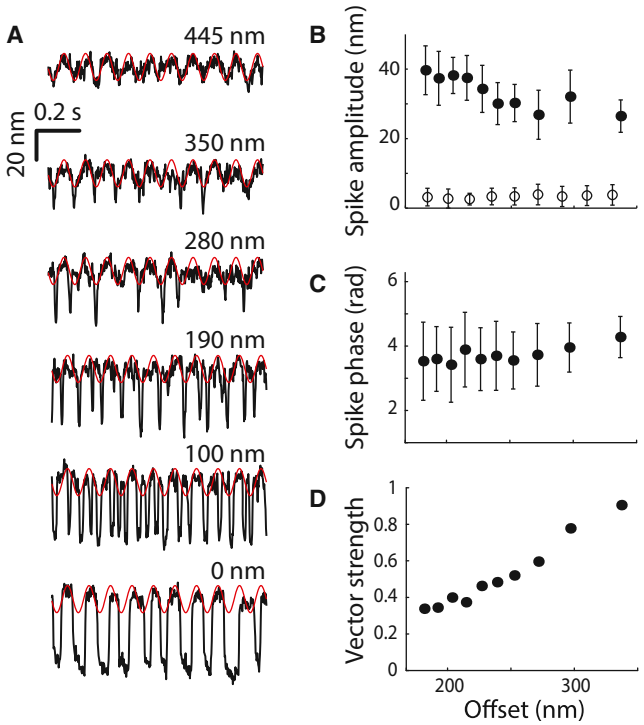

FIGURE 2 Phase-locking in the spiking regime. (*A*) Hair bundle oscillation measured at different offsets, with a sinusoidal stimulus of 15 nm amplitude applied at 10 Hz (*red lines*). (*B*) Spike amplitude (*solid circles*) and passive response (*open circles*). The passive response remained constant at ~3 nm. (*C*) Averaged spike phase saturated at ~1.5π rad at large offset. (*D*) Vector strength showed a rapid increase with offset in the spiking regime. Each point in *B* and *C*, represents the average of values obtained from 20 successive spikes, and error bars are the standard deviation.

Spikes evoked by mechanical stimuli

Next, we applied bursts of a 10-Hz sinusoidal stimulus, with amplitudes of 5, 10, and 20 nm applied to the base of the stimulus fiber, superposed onto slow ramps. As can be readily seen from the trace measured at 97–140 nm offset (Fig. 3 *A*), a regime could be observed where spikes only occurred during the application of a stimulus. This clearly illustrates that, in response to a mechanical signal, a quiescent hair bundle can exhibit amplified motion at preferred phases of the stimulus cycles via generation of spikes. The evoked spikes occurred at very large offsets, close to the suppression of active motility; significant variation was observed in the evoked spike amplitudes.

The number of spikes per unit time did not show an overall increase with respect to the spontaneous rate until stimuli of $\geq$20 nm in amplitude were imposed (Fig. 3 *B*). However, the vector strength in the spiking regime, calculated over the offset range near the suppression of active motility (~180 nm), showed a significant improvement upon application of even very weak signals (5 nm) (Fig. 3 *C*). In contrast, comparable enhancement of phase-locking in the oscillatory regime required a higher stimulus amplitude (10 nm or higher). Hence, the spiking regime proved to be more sensitive to entrainment by mechanical stimuli. The vector strength at different bundle offsets is shown in Fig. S4.

Active work performed by a hair bundle

We calculated work done by a hair bundle during a spike. Power delivered by the hair bundle ($-P_{\mathrm{d}} - P_{\mathrm{sf}}$) was defined as the difference between the dissipated power (P_{d}) generated by the bundle in overcoming the drag force and the power delivered by the stimulus fiber (P_{sf}) (see Supporting Material for details of the calculation) (14). For spontaneous spikes, active work was then obtained from integrating $-P_d - P_{sf}$ over the course of a spike, defined as the interval from 10 ms before to 10 ms after the threshold crossing, corresponding to the onset and the cessation of a spike, respectively. The calculation indicated that, during the occurrence of a spontaneous spike (Fig. 4 *A*), the work performed by the bundle in overcoming dissipation exceeded the work performed on the bundle by the stimulus fiber, corresponding to net positive active work. This suggests that spike occurrence requires an active mechanism. At the onset of the spontaneous spiking regime, total active work done by the

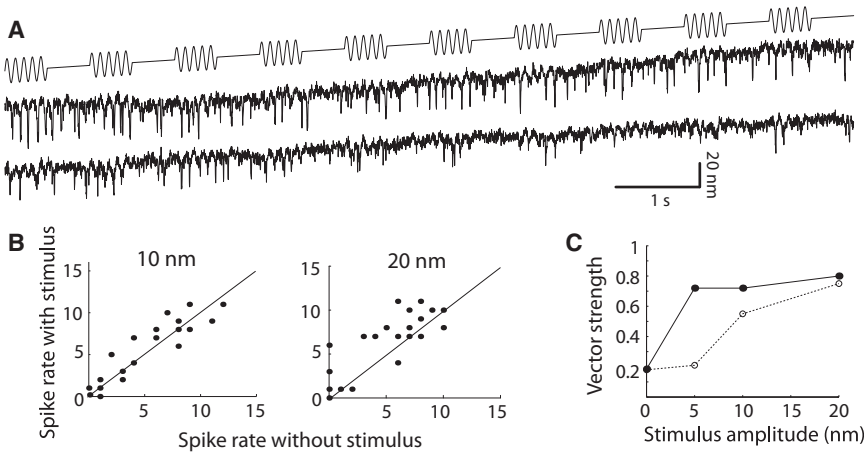

FIGURE 3 Effects of stimulus amplitude. (*A*) Hair bundle oscillations with bursts of applied 20 nm stimulus (*upper trace*). The offsets varied from 45 to 97 nm (*middle trace*) and from 97 to 140 nm (*lower trace*). (*B*) Comparison of the number of spikes per stimulus cycle with versus without an imposed stimulus, obtained at 10 and 20 nm stimulus amplitudes. Data were obtained from the spiking regime only. The 20-nm stimulus clearly increased the number of spikes at any offset. (*C*) Vector strength of spike phase in the spiking (*solid circles*) and oscillatory (*open circles*) regimes at 5-, 10-, and 20-nm stimulus amplitudes. Data were obtained at ~180 nm offset.

bundle per spike was ~70 zJ, slightly below that of the total active work performed per cycle in the oscillatory regime (~100 zJ, data not shown). At larger offset, active work per spike shows a slight decrease to ~40 zJ. Calculation of the power delivered at any instant during a spontaneous spike, near the suppression of active motility (Fig. 4 *C*, at 140 nm offset), showed that over the course of the channel closing, the bundle generated active work of ~70 zJ. Restoring force exerted by the elastic glass fiber assisted channel reopening, during which the bundles performed a net negative work of ~−20 zJ.

In the presence of a sinusoidal stimulus, $-P_d - P_{sf}$ was integrated over the period of each stimulus cycle to obtain active work. At the onset of the spiking regime, the total active work performed by the bundle per stimulus cycle, with spikes generated, was ~50–60 zJ (Fig. 4 *B*, *solid*

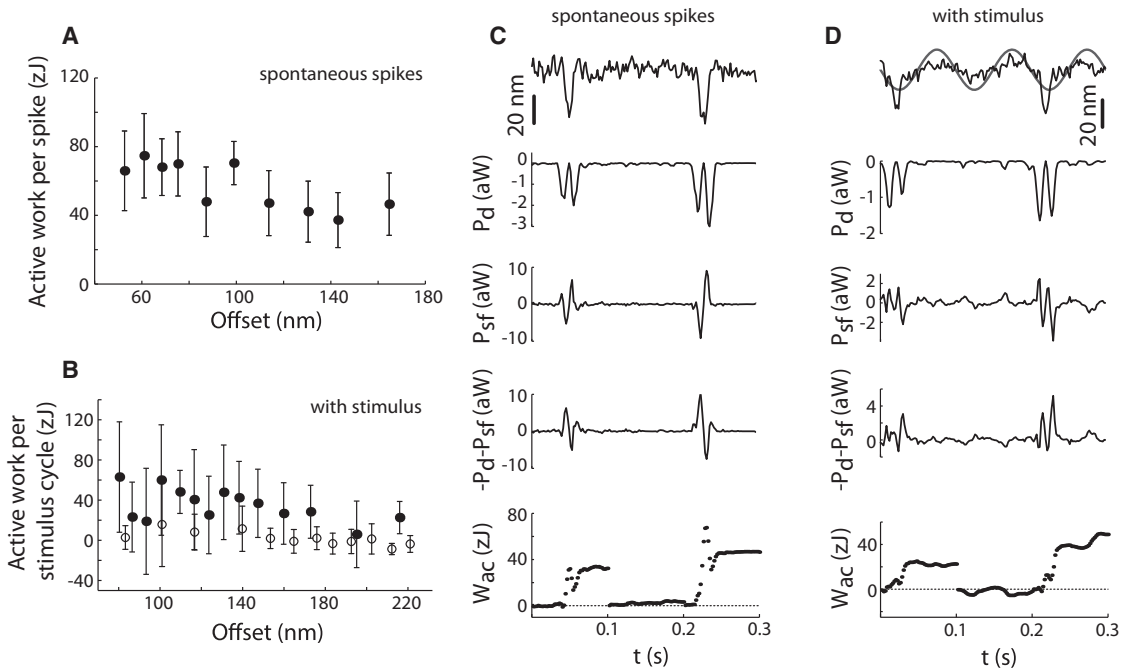

FIGURE 4 Calculation of active work performed by a hair bundle. (*A*) Active work done by the hair bundle during each spontaneous spike at different offsets, calculated from data shown in Fig. 1 *A*. Each point represents the average of values obtained from 10 successive spikes, and error bars are the standard deviation. (*B*) Active work performed by the hair bundle in the presence of 15-nm sinusoidal stimulus at 10 Hz, calculated from data shown in Fig. 2 *A*. Each point represents the average of values obtained from 10 successive stimulus cycles with (*solid circles*) and without (*open circles*) spikes observed. (*C*) Hair-bundle motion during spontaneous spikes at 140 nm offset (*upper trace*), power from the viscous drag (P_d), power delivered from the stimulus fiber (P_{sf}), power delivered by the hair bundle ($-P_d - P_{sf}$), and active work performed by the bundle during each spike (W_{ac}), integrated over each 0.1-s window. (*D*) Hair-bundle motion during entrained spikes at 200 nm offset with 15-nm stimulus at 10 Hz (*upper trace*, *gray line*), P_d, P_{sf}, $-P_d - P_{sf}$, and W_{ac} calculated over each stimulus cycle (0.1-s window).

circles), then decayed to ~20 zJ at large offsets. For stimulus cycles without spikes generated (only the passive response), active work was ~ 0 zJ (Fig. 4 *B*, *open circles*). Note, however, that at large offsets, where evoked spikes were observed, the bundle generated positive active work during both channel closing and reopening excursions (Fig. 4 *D* and Fig. S5).

Spikes at different stimulus amplitudes

To explore amplification by a hair bundle in the quiescent state, we applied a large static offset (~0.6 μm at the base of the probe, corresponding to ~100 pN) to the tip of the bundle, in the positive direction, to suppress active motility. Typical deflections of the tips of the bundles due to the applied offset were ~200–300 nm. To avoid the effects of long-term adaptation, the offset was applied as a square wave, with the bundle returning to the original position upon cessation of each sinusoidal stimulus train. We examined the effects of increasing amplitudes (3, 4, 8, 10, 12, 14, 16, 20, 30, 40, 50, 70, and 100 nm) on the bundle response (Fig. 5 *A*). The order of stimuli presented was randomized to avoid any consistent cumulative effects of adaptation.

We decomposed the response of the bundle and measured separately the amplitude of the passive response and the amplitudes of the superposed spikes. We found that the spike amplitude remained largely constant, with a slight increase at very large stimuli, whereas the passive response increased linearly with the stimulus amplitude (Fig. 5 *B*). The number of spikes per stimulus cycle gradually increased with signal amplitude, with the increase well described by a Boltzmann curve, with thresholds between 60 and 100 nm, which varied among cells. The vector strength, on the other hand, increased rapidly at small stimuli (~10–20 nm), and saturated at ~0.9 for stimuli >20 nm (Fig. 5 *C*).

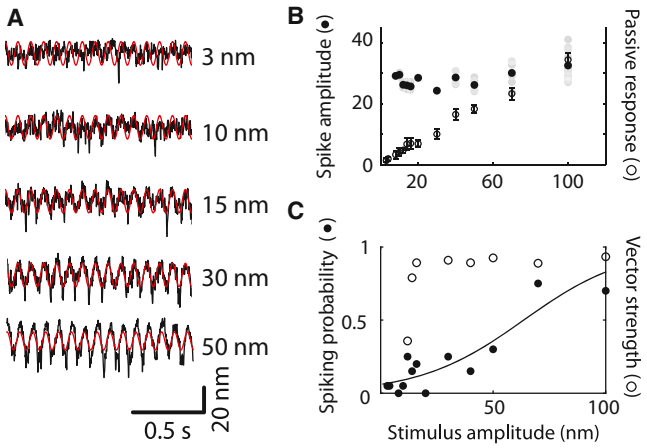

FIGURE 5 Mechanical amplification by a quiescent hair bundle at different signal amplitudes. (*A*) Hair-bundle motion in the quiescent state with different amplitudes of the imposed stimulus (3, 10, 15, 30, and 50 nm). Stimuli of 10 Hz were superposed in red lines (not to scale). (*B*) Averaged spike amplitude (*solid circles*) and passive response (*open circles*) as a function of the stimulus amplitude. Individual spike amplitudes are shown as gray dots. (*C*) Vector strength (*open circles*) and the number of spikes per stimulus cycle (*solid circles*). The solid line shows a Boltzmann fit to the spiking probability.

By observing the passive response and the spike amplitude separately, we can define an amplitude gain due to the spiking as the ratio of spike amplitude to passive movement. The amplitude gain was highest at small stimulus amplitudes, reaching a 100-fold increase, and dropped off with increasing stimuli (Fig. 6 *A*). The power-law exponent was ~−1, as the spike amplitude remained constant. Calculation of the active work generated per spike showed a significant reduction upon increasing stimulus amplitude, with zero crossing occurring at ~40–80 nm (Fig. 6 *B*), corresponding to ~6–12 pN of force applied to the bundle. This indicated the range of stimulus amplitudes above which the hair bundle no longer amplified. This amplification cutoff corresponded to spike probability of ~0.3–0.5 (Fig. 6 *C*). Hence, amplification of motion occurs when spiking is a relatively rare event.

Not only did the spike amplitude remain largely constant over a wide range of stimulus amplitudes, it also did not show much variation with stimulus frequency (Fig. S6). The vector strength of spike phase fluctuated about a constant value over a wide range of stimulus frequencies (5–100 Hz).

Numerical simulations

We performed numerical simulations to explore the underlying mechanisms of bundle motility in the spiking regime. The numerical model used in this study, as explained in Roongthumskul et al. (26) and based on studies by Martin and colleagues (8,27), describes spontaneous oscillations as an interplay between channel gating and the adaptation process due to myosin 1c motors (see Supporting Material). The model can reproduce the spiking regime (Fig. 1 *E*), with the slow reduction in spike amplitude due to the existence of a variable gating spring—an internal spring with a calcium-dependent stiffness whose dynamics are slow with respect to those of the myosin motors.

Based on the numerical model, the dynamics of a hair bundle can be described by using a double-well potential, corresponding to channel opening and closing states. Adaptation activity imposes an increasing tilt on the energy landscape, promoting channel opening or closing. This tilting of the double-well potential corresponds to the shift of the force-displacement curve along a sloped line (28).

At the onset of the spiking regime, at moderate deflections, the adaptation process is required for spike generation. Before a spike, the bundle resides in a shallow local minimum in the channel opening state. A small perturbation due to noise or an external stimulus promotes the system to overcome the barrier and leads to the channel closing excursion. Adaptation then plays a role to modify the energy

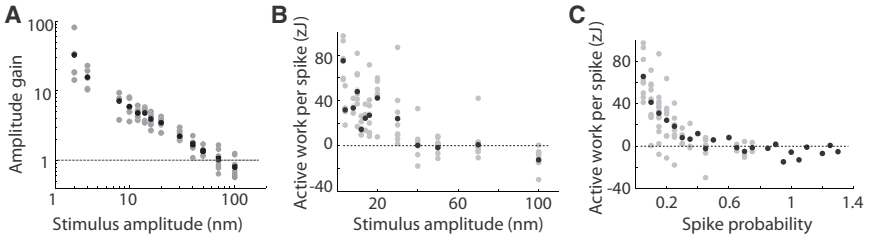

FIGURE 6 Mechanical amplification by quiescent hair bundles. Black circles indicate the averaged and gray circles indicate the individual values. Data were obtained from 10 bundles. (*A*) Amplification gain at different stimulus amplitudes, defined as the ratio between the spike amplitude and the passive response. Dashed line indicates gain of unity. (*B* and *C*) Active work per spike evoked by the stimulus as a function of stimulus amplitude (*B*) and spike probability (*C*). Dashed lines indicate zero active work.

landscape until the channel closing state becomes unstable, leading to reopening of the channels (Fig. 7 *A*).

As the bundle is further deflected into the spiking regime and away from the oscillatory regime, the channel opening state becomes the global minimum (Fig. 7 *B*). Small external stimulus or thermal fluctuations can excite the system across the energy barrier to a local minimum, causing channel closing. Channel reopening then occurs spontaneously; the effects of adaptation process are minimal or absent, particularly when the channel closing state is unstable at very large offsets. This agrees with experimental observations of spike duration, which is too short for myosin motors to exert much effect (~10 ms). Spontaneous activity was completely suppressed when the energy barrier was too large (~2–3 k_BT, variable among cells).

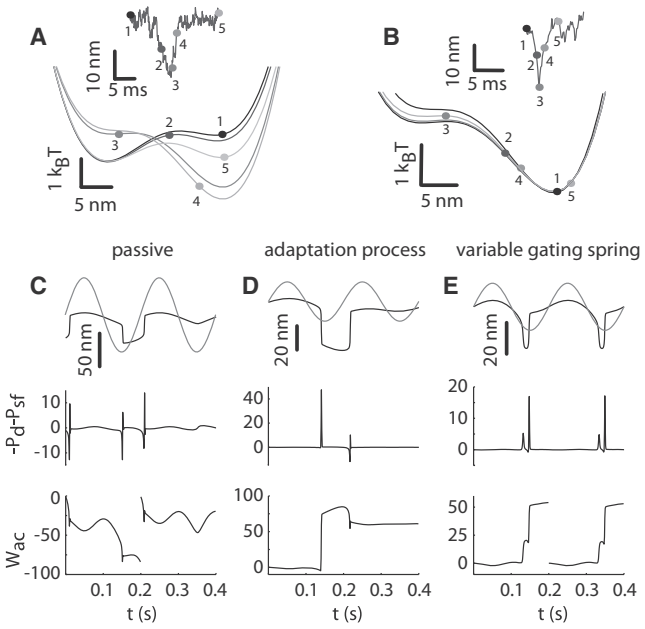

FIGURE 7 Numerical simulations. (*A*) Energy landscapes corresponding to different states of a bundle over the duration of a spontaneous spike at time points indicated in the inset. Adaptation plays a crucial role in modifying the stability of the system. Simulations were performed at a moderate steady-state deflection. (*B*) Energy landscapes corresponding to different states of a bundle during a noise-induced spontaneous spike (*inset*). Effects of the adaptation process were minimal, and reopening of the channel occurred due to the instability of the channel closing state. (*C–E*) Evoked spikes with sinusoidal stimulus at 5 Hz. (*Upper traces*) Hair-bundle motion during evoked spikes (*black traces*), and stimulus applied to the base of the fiber (*gray traces*). (*Middle traces*) $-P_d - P_{sf}$. (*Lower traces*) Active work calculated over a stimulus period (0.2-s window). (*C*) A passive hair bundle, with no adaptation process and constant gating-spring stiffness (800 μN/m). Stimulus amplitude is 55 nm. (*D*) A hair bundle with only the adaptation process included. (*E*) A hair bundle with only the variable gating spring included.

Further results from simulations of a quiescent bundle under large positive offset showed that a passive bundle, for which the adaptation rate was set to zero (Eq. S4) and the gating spring stiffness was a constant, can also exhibit evoked spikes upon the application of a large stimulus (>50 nm), as shown in Fig. 7 *C* (*upper*). This suggests that gating of the transduction channels alone is sufficient for the occurrence of spikes. However, due to the power delivered by the glass fiber, the net work generated by the bundle was found to be negative (~−90 zJ); the system was hence dissipative, as expected in the absence of an active process. Incorporating either the adaptation process or a variable gating spring in the model led to active bundle motility during spikes, with positive net work performed. Further, the threshold for evoking spikes was significantly reduced to a stimulus of <10 nm. Including a 15-nm stimulus in the numerical models that included only the adaptation process or only a variable gating spring yielded active work per spike of ~60 zJ and ~55 zJ, respectively (Fig. 7, *D* and *E*). This suggested that either the variable gating spring or the adaptation motors can be an effective source of power. However, rapid spikes (~10–20 ms, as observed in experimental data) can only be achieved in the presence of a variable gating spring, regardless of the presence of an adaptation process. Further, the bundle generated positive active work during both channel closing and opening, as observed in the experimental data (Fig. 4 *D*).

DISCUSSION

A number of in vivo studies have demonstrated the presence of an amplification process in the inner ear, and yet its precise cellular mechanism remains a subject of ongoing study (4,6,29,30). In nonmammalian species, amplification of an applied signal has been demonstrated in vitro in spontaneously oscillating hair bundles (14). This amplification occurred through the entrainment of an innate large-amplitude limit-cycle oscillation by a smaller sinusoidal stimulus.

The response exhibited a compressive nonlinearity, consistent with theoretical predictions, and weak frequency selectivity, consistent with the characteristics of the amphibian sacculus (10). However, there are thus far no observations of spontaneous oscillation under in vivo conditions. Even in vitro, these oscillations are absent when the natural loading by the overlying otolithic membrane is maintained. Hence, a question that has remained open is how these cells might amplify a signal if their innate oscillations are suppressed.

The occurrence of spikes exhibited by hair bundles under mechanical offset constitutes a potential amplification mechanism for hair bundles that are poised in the quiescent regime. Calculation of work done by a quiescent hair bundle in response to a weak stimulus indicates that the system performed active work via the generation of spikes. However, due to low spiking probability, only a fraction of hair bundles in the sacculus would exhibit spikes in response to one stimulus cycle. At larger stimulus amplitudes, more bundles exhibit spikes, but the system is rendered more dissipative.

The characteristics of spiking behavior shown here are consistent with theoretical studies of hair bundle motility (18,31). In a recent study, hair cell motion was modeled with a time-dependent Adler equation, which describes a system moving in a tilted washboard potential. The addition of an offset term leads to a time-dependent modulation of the barrier height. It was shown that such a model leads to the occurrence of spikes, which can be entrained by a weak signal (31). Our data confirm the existence of spikes, and show that this entrainment occurs at extremely weak signals, before any effects on spike amplitude or rate are observed.

Our numerical model shows that the mechanism responsible for the sharp excursions is the sudden closure and reopening of the transduction channels. Although at least one active mechanism is required for the production of net work by the bundle, the model indicates that the adaptation process, mediated by myosin 1c, plays a minimal role in the occurrence of spikes in the regime near the suppression of active motility.

SUPPORTING MATERIAL

Supporting Materials and Methods, ten equations, seven figures, and one table are available at http://www.biophysj.org/biophysj/supplemental/S0006-3495(14)01192-8.

ACKNOWLEDGMENTS

This work was supported in part by the National Science Foundation (grant CMMI-1131842) and the National Institutes of Health (grant RO1DC011380).

SUPPORTING CITATIONS

References (31,32) appear in the Supporting Material.

REFERENCES

1. Hudspeth, A. J. 2000. Hearing. *In* Principles of Neural Science. J. H. Kandel, E. R. Schwartz, and T. M. Jessell, editors. McGraw Hill, New York, pp. 590–624.
2. Robles, L., and M. A. Ruggero. 2001. Mechanics of the mammalian cochlea. *Physiol. Rev.* 81:1305–1352.
3. van Netten, S. M., T. Dinklo, …, C. J. Kros. 2003. Channel gating forces govern accuracy of mechano-electrical transduction in hair cells. *Proc. Natl. Acad. Sci. USA.* 100:15510–15515.
4. Dallos, P. 2008. Cochlear amplification, outer hair cells and prestin. *Curr. Opin. Neurobiol.* 18:370–376.
5. Dallos, P., X. Wu, …, J. Zuo. 2008. Prestin-based outer hair cell motility is necessary for mammalian cochlear amplification. *Neuron.* 58:333–339.
6. Fettiplace, R. 2006. Active hair bundle movements in auditory hair cells. *J. Physiol.* 576:29–36.
7. Martin, P. 2008. Active hair-bundle motility of hair cells of vestibular and auditory organs. *In* Active Process and Otoacoustic Emission. G. A. Manley, R. R. Fay, and A. N. Popper, editors. Springer, New York, pp. 93–143.
8. Martin, P., D. Bozovic, …, A. J. Hudspeth. 2003. Spontaneous oscillation by hair bundles of the bullfrog's sacculus. *J. Neurosci.* 23:4533–4548.
9. Crawford, A. C., and R. Fettiplace. 1985. The mechanical properties of ciliary bundles of turtle cochlear hair cells. *J. Physiol.* 364:359–379.
10. Martin, P., and A. J. Hudspeth. 2001. Compressive nonlinearity in the hair bundle's active response to mechanical stimulation. *Proc. Natl. Acad. Sci. USA.* 98:14386–14391.
11. Eguíluz, V. M., M. Ospeck, …, M. O. Magnasco. 2000. Essential nonlinearities in hearing. *Phys. Rev. Lett.* 84:5232–5235.
12. LeMasurier, M., and P. G. Gillespie. 2005. Hair-cell mechanotransduction and cochlear amplification. *Neuron.* 48:403–415.
13. Vollrath, M. A., K. Y. Kwan, and D. P. Corey. 2007. The micromachinery of mechanotransduction in hair cells. *Annu. Rev. Neurosci.* 30:339–365.
14. Martin, P., and A. J. Hudspeth. 1999. Active hair-bundle movements can amplify a hair cell's response to oscillatory mechanical stimuli. *Proc. Natl. Acad. Sci. USA.* 96:14306–14311.
15. Roongthumskul, Y., R. Shlomovitz, …, D. Bozovic. 2013. Phase slips in oscillatory hair bundles. *Phys. Rev. Lett.* 110:148103.
16. Camalet, S., T. Duke, …, J. Prost. 2000. Auditory sensitivity provided by self-tuned critical oscillations of hair cells. *Proc. Natl. Acad. Sci. USA.* 97:3183–3188.
17. Han, L., and A. B. Neiman. 2010. Spontaneous oscillations, signal amplification, and synchronization in a model of active hair bundle mechanics. *Phys. Rev. E Stat. Nonlin. Soft Matter Phys.* 81:041913.
18. Ó Maoiléidigh, D., E. M. Nicola, and A. J. Hudspeth. 2012. The diverse effects of mechanical loading on active hair bundles. *Proc. Natl. Acad. Sci. USA.* 109:1943–1948.
19. Pikovsky, A., M. Rosenblum, and J. Kurths. 2001. Synchronization: A Universal Concept in Nonlinear Sciences. Cambridge University Press, Cambridge, United Kingdom.
20. Kachar, B., M. Parakkal, and J. Fex. 1990. Structural basis for mechanical transduction in the frog vestibular sensory apparatus: I. The otolithic membrane. *Hear. Res.* 45:179–190.
21. Benser, M. E., N. P. Issa, and A. J. Hudspeth. 1993. Hair-bundle stiffness dominates the elastic reactance to otolithic-membrane shear. *Hear. Res.* 68:243–252.
22. Fredrickson-Hemsing, L., C. E. Strimbu, …, D. Bozovic. 2012. Dynamics of freely oscillating and coupled hair cell bundles under mechanical deflection. *Biophys. J.* 102:1785–1792.
23. Benser, M. E., R. E. Marquis, and A. J. Hudspeth. 1996. Rapid, active hair bundle movements in hair cells from the bullfrog's sacculus. *J. Neurosci.* 16:5629–5643.

24. Eatock, R. A. 2000. Adaptation in hair cells. *Annu. Rev. Neurosci.* 23:285–314.

25. Castellano-Muñoz, M., S. H. Israel, and A. J. Hudspeth. 2010. Efferent control of the electrical and mechanical properties of hair cells in the bullfrog's sacculus. *PLoS ONE.* 5:e13777.

26. Roongthumskul, Y., L. Fredrickson-Hemsing, …, D. Bozovic. 2011. Multiple-timescale dynamics underlying spontaneous oscillations of saccular hair bundles. *Biophys. J.* 101:603–610.

27. Nadrowski, B., P. Martin, and F. Jülicher. 2004. Active hair-bundle motility harnesses noise to operate near an optimum of mechanosensitivity. *Proc. Natl. Acad. Sci. USA.* 101:12195–12200.

28. Le Goff, L., D. Bozovic, and A. J. Hudspeth. 2005. Adaptive shift in the domain of negative stiffness during spontaneous oscillation by hair bundles from the internal ear. *Proc. Natl. Acad. Sci. USA.* 102:16996–17001.

29. Hudspeth, A. J. 2014. Integrating the active process of hair cells with cochlear function. *Nat. Rev. Neurosci.* 15:600–614.

30. Avan, P., B. Büki, and C. Petit. 2013. Auditory distortions: origins and functions. *Physiol. Rev.* 93:1563–1619.

31. Shlomovitz, R., Y. Roongthumskul, …, R. Bruinsma. 2014. Phase-locked spiking of inner ear hair cells and the driven noisy Adler equation. *Interface Focus.* 4:20140022.

32. Denk, W., W. W. Webb, and A. J. Hudspeth. 1989. Mechanical properties of sensory hair bundles are reflected in their Brownian motion measured with a laser differential interferometer. *Proc. Natl. Acad. Sci. USA.* 86:5371–5375.